Pergamon

PII: S0301-9322(96)00063-8

Int. J. Multiphase Flow Vol. 23, No. 1, pp. 193–203, 1997

0301-9322/97 $17.00 + 0.00

BRIEF COMMUNICATION

AIR BUBBLE ENTRAINMENT IN OPEN CHANNELS: FLOW STRUCTURE AND BUBBLE SIZE DISTRIBUTIONS

H. CHANSON
Department of Civil Engineering, The University of Queensland, Brisbane QLD 4072, Australia

(Received 23 March 1996; in revised form 22 August 1996)

1. INTRODUCTION

Historically air–water flows in open channels were investigated for steep chute and dam spillway applications. Self-aeration in chutes (e.g. figure 1) was initially studied because of the bulking effect of entrained air (Falvey 1980). Further, the presence of air within the boundary layer reduces the shear stress between the flow layers and hence the shear force (Chanson 1994). Also it may prevent or reduce the damage caused by cavitation (Wood 1991). Self-aeration in open channels is recognised now for its significant contribution to the air–water transfer of atmospheric gases such as oxygen and nitrogen.

A substantial amount of experimental data was collected on both models and prototypes (e.g. Wood 1991; Chanson 1993). Few researchers (e.g. Volkart 1980) investigated the air–water flow structure and bubble size characteristics. These studies used photographic techniques and could picture only the near-sidewall region. In this paper, the air–water flow properties were investigated with a double-tip conductivity probe (25 μm tip diameter) scanned at 40 kHz per channel. The analysis of experimental data (table 1) provides new results on the air–water flow structure and on the air–water properties down flat-slope channels: air concentration and mean air–water velocity distributions, distributions of bubble chord length (section 3) and bubble frequency (section 4).

2. EXPERIMENTAL APPARATUS

2.1. Apparatus

New experiments were conducted an a 25 m long channel with a 4.0° slope. The flume (0.5 m wide) is made of planed wooden boards (roughness height: $k_s = 1$ mm). Waters are supplied by a pump, with a variable-speed electronic controller, enabling a fine discharge adjustment in a closed-circuit system. Flow to the flume is fed through a smooth convergent nozzle (1.7 m long) (figure 1). The nozzle exit is 30 mm high and 0.5 m wide. The measured contraction ratio is about unity (i.e. $d_0 = 30$ mm for all experiments). Further details on the channel and the full set of data were reported in Chanson and Cummings (1996).

2.2. Instrumentation

Clear-water velocities were measured with a Pitot tube (3.3 mm external diameter, 20 mm distance between tip and lateral holes).

Air–water velocity and air concentration distributions were recorded using a double-tip conductivity probe (figure 2). The probe consists of two identical tips with an internal concentric electrode ($\emptyset = 25$ μm) made of platinum and an external stainless steel electrode of 200 μm diameter. The tips are aligned in the flow direction and the distance between the tips

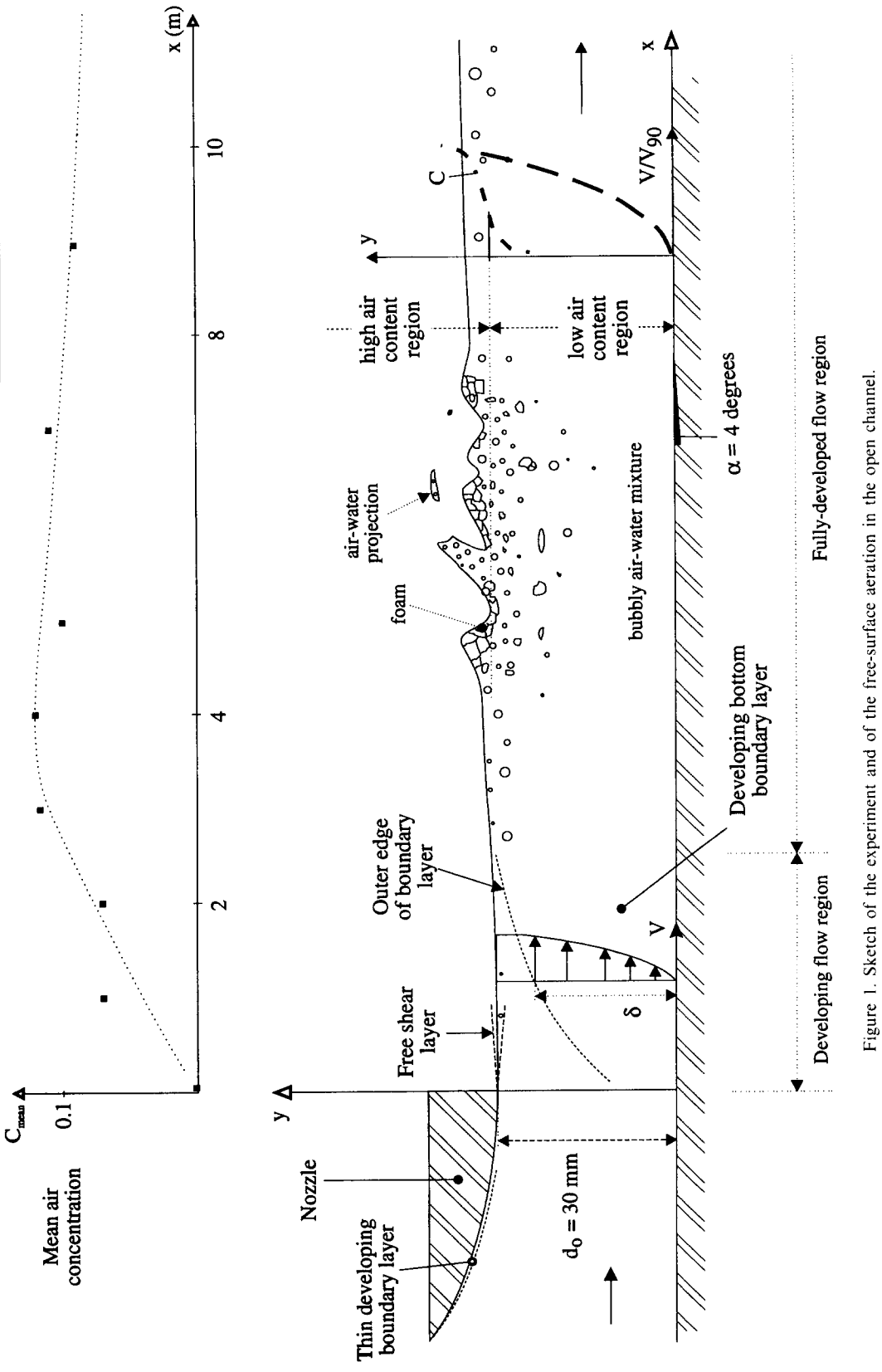

Figure 1. Sketch of the experiment and of the free-surface aeration in the open channel.

Table 1. Experimental flow conditions of air–water open channel flows

Ref. (1)	Slope α (deg.) (2)	q_w (m^2/s) (3)	V_{90} (m/s) (4)	Y_{90} (m) (5)	d_o (m) (6)	Comments (7)
Present study	4.0		3.4—5.5	0.03–0.045	0.03	$W = 0.5$ m. Flume length: 25 m. Painted timber ($k_s = 1$ mm)
		0.142†				Run MC2
		0.150†				Run P5
		0.150‡				Run PDC1
		0.156†				Run MC3
		0.164†				Run MC4
Thandaveswara (1974)	15.3–30.7	0.062–0.201	—	—	—	$W = 0.457$ m. Flume length: 13 m. Sand paper roughness: $k_s = 0.9$mm
Cain (1978)	45	2.23	18.1–20.4	0.18–0.26	0.3	Prototype spillway
		3.16	18.9–21.7	0.21–0.31	0.45	
Volkart (1980)	12	—	—	—	—	Partially-filled pipe flow. $\emptyset = 0.24$ m. Pipe length: 50 m
Chanson (1988)	52.33	0.265–0.40	10–17.8	0.04–0.056	—	Flow downstream of an aeration device. $W = 0.25$ m. Perspex flume

†Data reported in Chanson (1995). ‡Data reported in Chanson and Cumming (1996). §Estimated by the author. — Information not available.

is 7.42 mm (figure 2). Both tips are excited by an air bubble detector (DSIR AS25240). This electronic system was designed with a response time less than 10 μs and it was calibrated with a square wave generator.

The vertical translation of the probe was controlled by a fine adjustment travelling mechanism connected to a digimatic scale unit. The error on the vertical position of the probe was less than 0.025 mm. The system (probe and travelling mechanism) was mounted on a trolley travelling parallel to the channel bottom. The accuracy on the longitudinal position of the probe was estimated as $\Delta x = 1$ cm.

2.3. *Data processing*

At each position $\{x,y\}$ the two tip signals from the conductivity probe were recorded with a scan rate of 40 kHz per channel for a 5.12 s scan period. The air concentration C (or void fraction) was computed as the probability of encountering air at the leading tip of the probe. The calculations were based on a 50% threshold between air and water. The mean air–water velocities V were computed using a cross-correlation technique. The cross-correlation function between the two tip signals is maximum for the average time taken for an air–water interface to travel from the first tip to the second tip. The velocity is deduced from the time delay between the signals and the tip separation distance.

The bubble chord length† distributions were also deduced. Chord length calculations assumed that the bubble velocity equalled the local mean air–water velocity (i.e. no slip between air and water phases). The number of detected bubbles N_{ab} was also recorded. Note that an "air bubble" is defined as a volume of air (i.e. air entity) detected by the leading tip of the probe between two consecutive air–water interface events. The flow field was investigated for void fractions between 0 and 90%. As in the region of high-air content, the structure of the air–water mixture is extremely complex (see section 4), only bubble chord length data are presented here.

2.4. *Developing flow region*

In the upstream section of the channel, transverse velocity profiles were recorded immediately downstream of the nozzle (Chanson 1995). They showed that the velocity distributions were uniform.

†The bubble chord length is the length of straight line connecting the two intersections of the air bubble free-surface with the leading tip of the probe as the bubble is transfixed by the probe sharp-edge.

At the upstream end of the chute, a turbulent boundary layer is generated by the channel bottom (figure 1). Clear-water velocity measurements suggested consistently a boundary layer growth which differs with the boundary layer development along a flat plate (e.g. Schlichting 1979). The analysis of the data indicates that the growth of the boundary layer thickness δ is best correlated by:

$$\frac{\delta}{k_s} = 1.0196 \times 10^{-2} \left(\frac{x}{k_s} + 757 \right)^{0.973} \quad [1]$$

with a coefficient of correlation of 0.99895, where k_s is the equivalent roughness height and x is the distance from the nozzle exit. Equation [1] is of similar form as wall jet experimental results: e.g. Schwarz and Cosart (1964) observed $\delta/k_s = 0.0678\ (x + 0.2838)/k_s$ for wall jet experiments in a wind tunnel.

The bubble chord length measurements were performed at three particular cross-sections ($x = 4$, 12 and 23 m). At each location the flow field was fully-developed and air bubble entrainment was substantial.

3. EXPERIMENTAL RESULTS

3.1. *Mean air–water flow properties*

Distributions of air concentration and mean velocities were measured at various centreline positions (from $x = 0.05$–23 m). Typical results are plotted, respectively, in figures 3 and 4 as C and V/V_{90} as functions of y/Y_{90} where y is the distance normal to the channel bottom, Y_{90} is the characteristic distance where $C = 0.9$ and V_{90} is the velocity at Y_{90}.

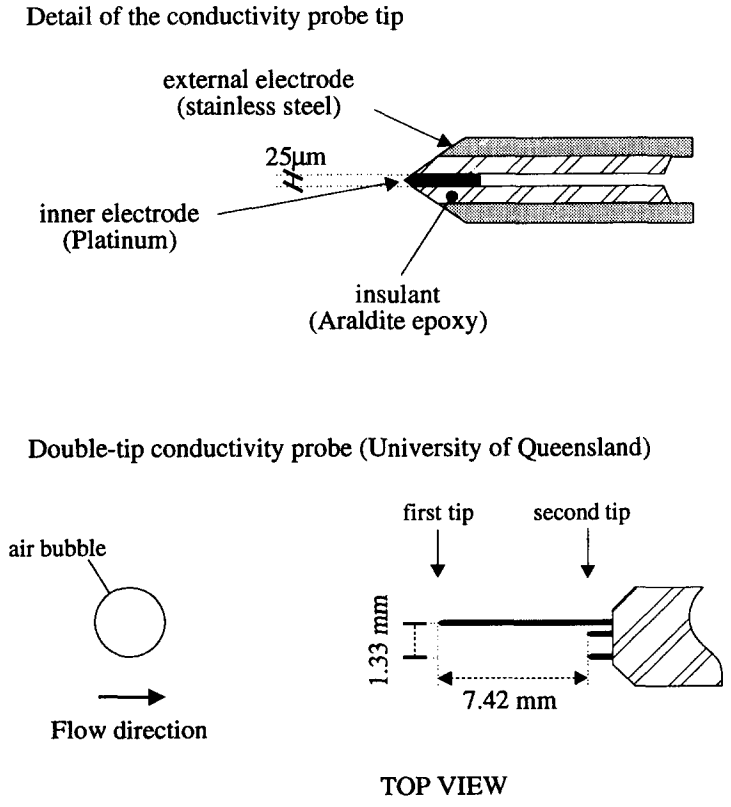

Figure 2. Sketch of the double-tip conductivity probe developed at the Hydraulics/Fluid Mechanics Laboratory of the University of Queensland.

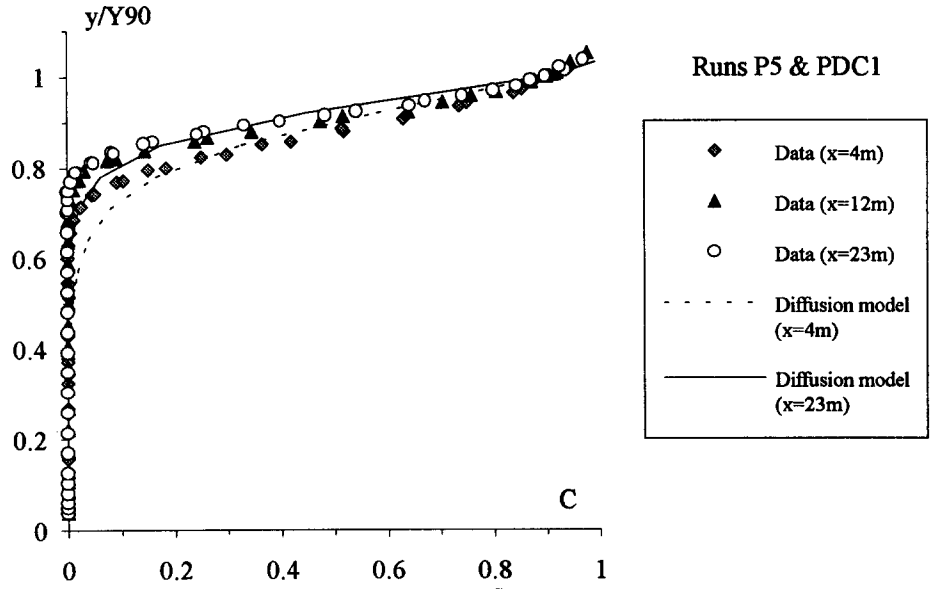

Figure 3. Air concentration distributions—comparison with an air bubble diffusion model (Chanson 1995). Runs P5 and PDC1, $q_w = 0.15$ m^2/s, $d_o = 0.03$ m.

Both the air concentration and velocity distributions exhibit smooth continuous curves from 0 to 90% of air content. They indicate no discontinuity within the flowing mixture, exphasising a homogeneous mixture flow.

The void fraction profile can be fitted with simple diffusion models (e.g. Wood 1991; Chanson 1995) as shown in figure 3. The velocity data follow closely a 1/6th power law as for earlier data (Cain 1978; Chanson 1988). Although the velocity distribution follows a logarithmic law in fully-developed open channel flows, it is more consistent with the scatter of data to compare the results with a simple power law function as shown in figure 4. Note that, on figure 4, the scatter of points differs between prototype (Cain 1978) and model data (Chanson 1988; present study) because of the different accuracy of the instrumentation.

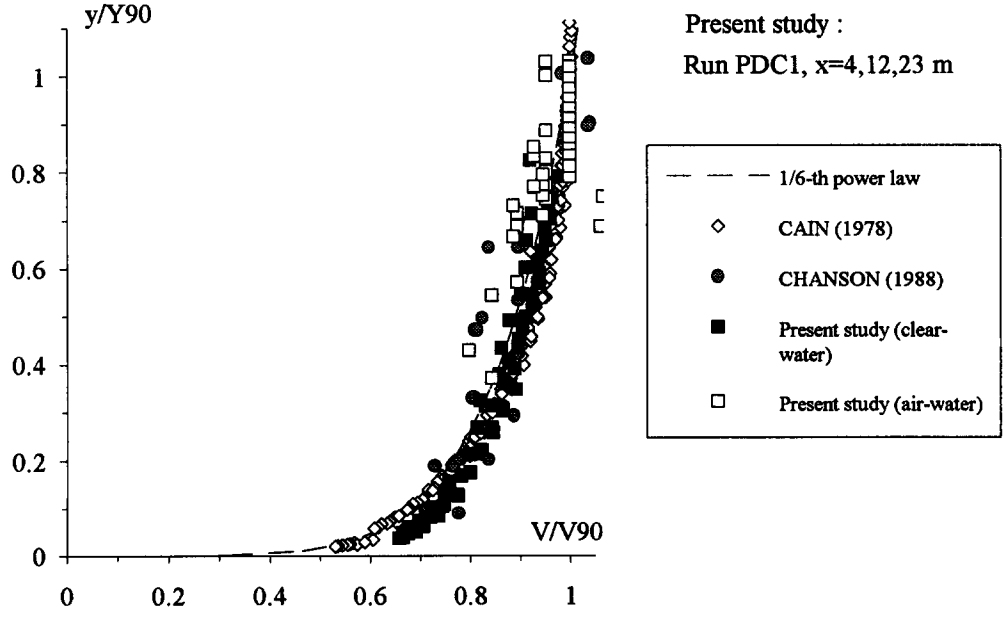

Figure 4. Dimensionless velocity distributions in air–water open channel flows—comparison between model data (Chanson 1988, present study) and prototype data (Cain 1978).

(A) Run PDC1, x = 4 m, Y_{90} = 0.035 m, V_{90} = 5.03 m, C_{mean} = 0.123, Δch_{ab} = 1 mm (unless specified)

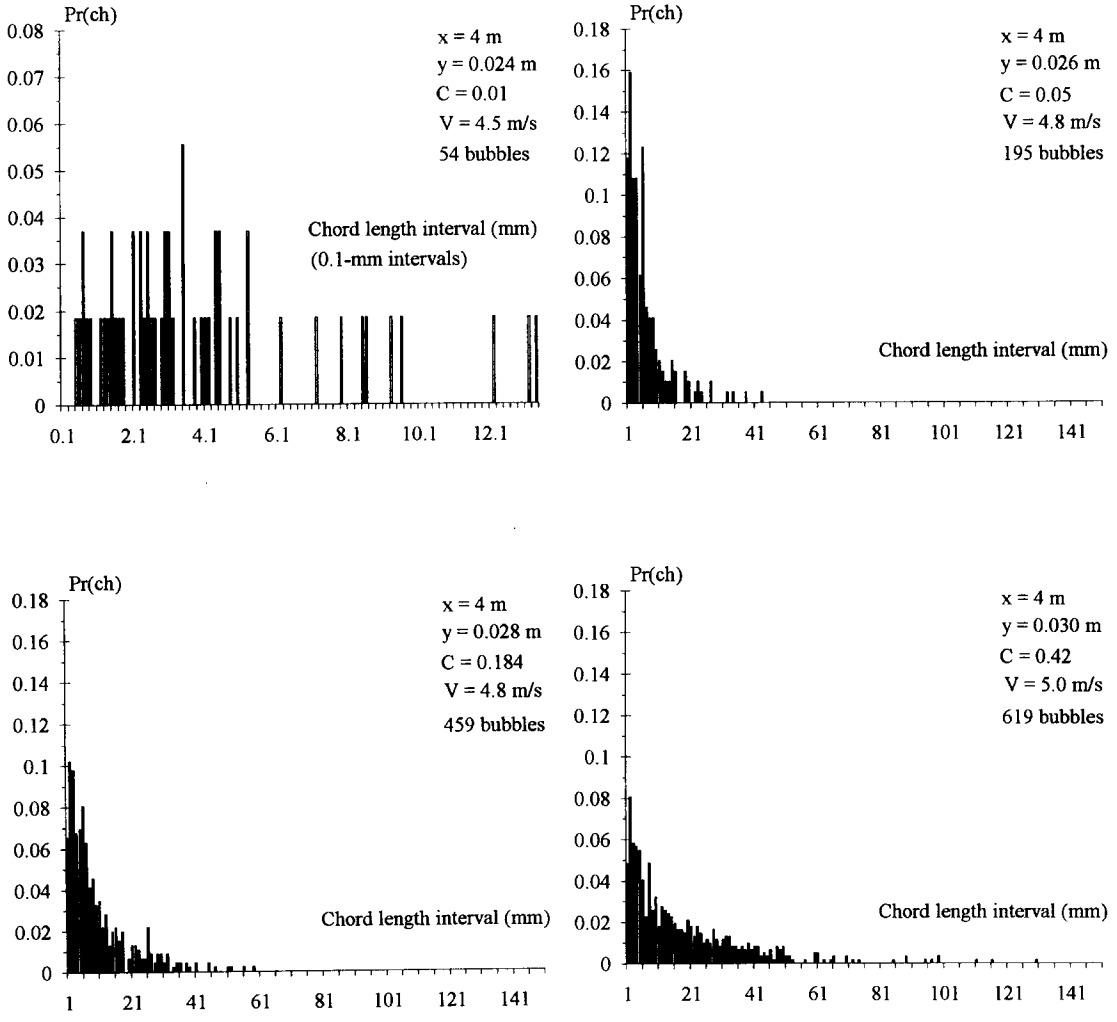

Fig. 5—*Caption opposite*

3.2. Chord length distributions

Figure 5 shows bubble chord distributions at various $\{x,y\}$ positions along the flume. For each figure, the caption provides the local air–water flow properties (C, V), the number of detected air bubbles N_{ab} during the scan period (t = 5.12 s) and the bubble chord length interval Δch_{ab}. The histogram columns represent each the probability of a bubble chord length in a Δch_{ab}-interval, e.g. with Δch_{ab} = 1 mm, the probability of bubble chord length from 2 to 3 mm is represented by the column labelled 3 mm.

First note the broad spectrum of bubble chord lengths at each location $\{x,y\}$. The range of bubble chord length extends over several orders of magnitude including at low air contents.

Secondly the distributions are skewed with a preponderance of small bubble sizes relative to the mean. Figure 5 suggests also that the probability of bubble chord lengths is the largest for chord lengths between 0 and 3 mm.

Thirdly let us observe that the bubble chord length distributions have a similar shape in both high- and low-air-content regions although the air–water structures differ substantially (see next section). Note also that the maximum bubble chord length increases consistently as the air concentration and the distance from the bottom increase.

4. DISCUSSION

4.1. *Structure of the bubbly flow region*

In open channel flows, measurements (e.g. figures 3 and 4) indicate that the air–water flow behaves as a homogeneous mixture for $C < 0.90$. The bubble rise velocity component in the flow direction is indeed very small. In the air–water flow, high-speed photographs and conductivity probe records suggest two air–water regions: a bubbly flow region for low air contents and a highly-aerated flow mixture for $C > 0.3$–0.4 (figure 1). In the bubbly region (i.e. $C < 0.3$–0.4) the homogeneous mixture comprises individual air bubbles of irregular shapes, cluster of air bubbles and air packets surrounded by a continuous liquid medium. Several researchers photographed such a bubbly flow structure (e.g. Halbronn *et al.* 1953; Straub and Lamb 1953).

In the highly-aerated flow (i.e. $C > 0.3$–0.4), the flow structure becomes more complex. Two types of air–water structures co-exist quasi-simultaneously: air–water projections and foam (e.g. Thandaveswara 1974; Volkart 1980). Air–water projections are irregularly ejected away from the main mixture flow. Volkart (1980) showed superb examples. The projections are highly-aerated. Foam structures are also observed. The emulsion consists of large air clusters separated by film interfaces, gliding smoothly over the outer edge of the homogeneous flow. The "bubble" shape is basically pentagonal to decahedronal. Both air–water projections and foam structures are instantaneous structures which constantly evolve in shapes and sizes with time.

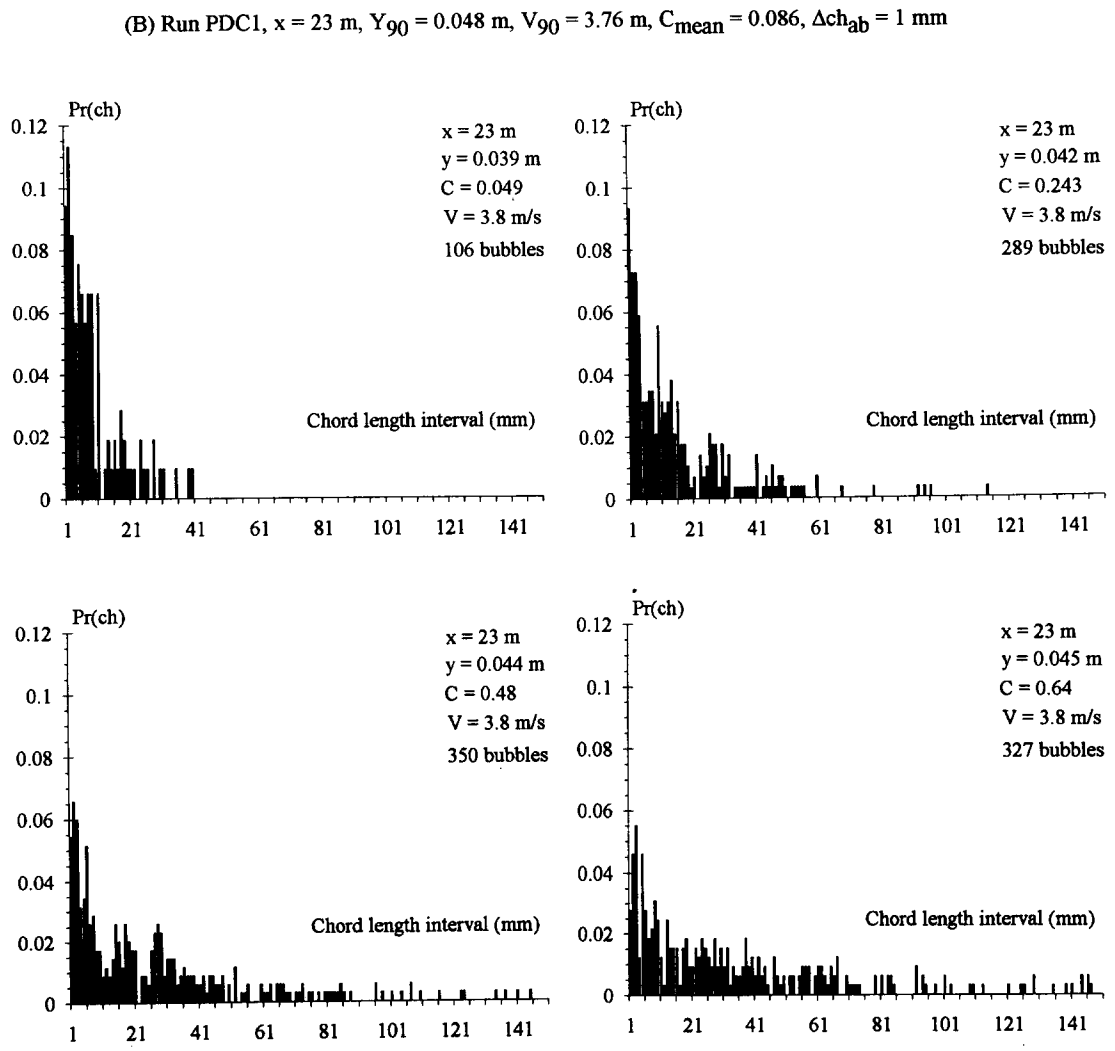

Figure 5. Air bubble chord length distributions.

(A) Bubbly flow region ($C < 0.30$) : $0 < y < 0.0426$ m

$N_{ab} = 808$, $(ch_{ab})_{NMS} = 0.0127$ m, $(ch_{ab})_{max} = 0.190$ m

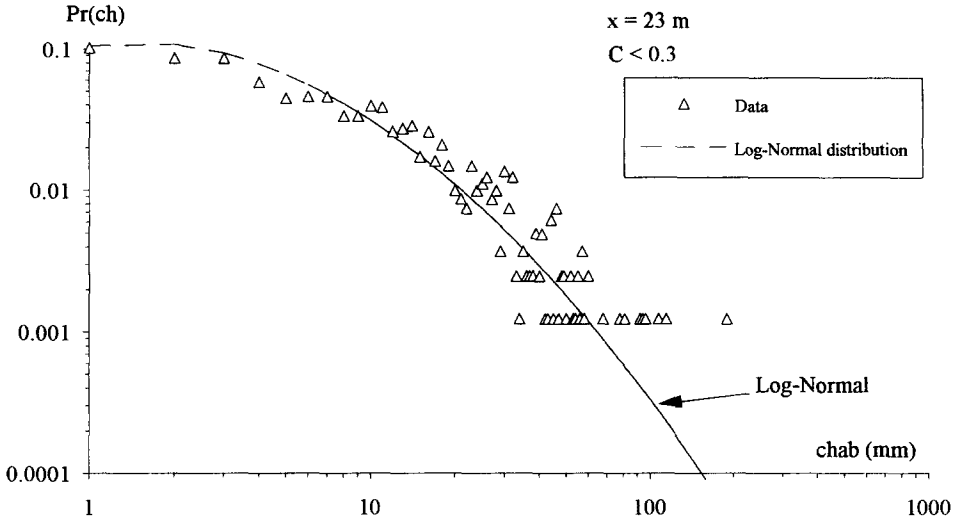

(B) High air content region ($0.9 > C > 0.30$) : $0.0426 < y < 0.0481$ m

$N_{ab} = 1605$, $(ch_{ab})_{NMS} = 0.0335$ m, $(ch_{ab})_{max} = 1.4395$ m

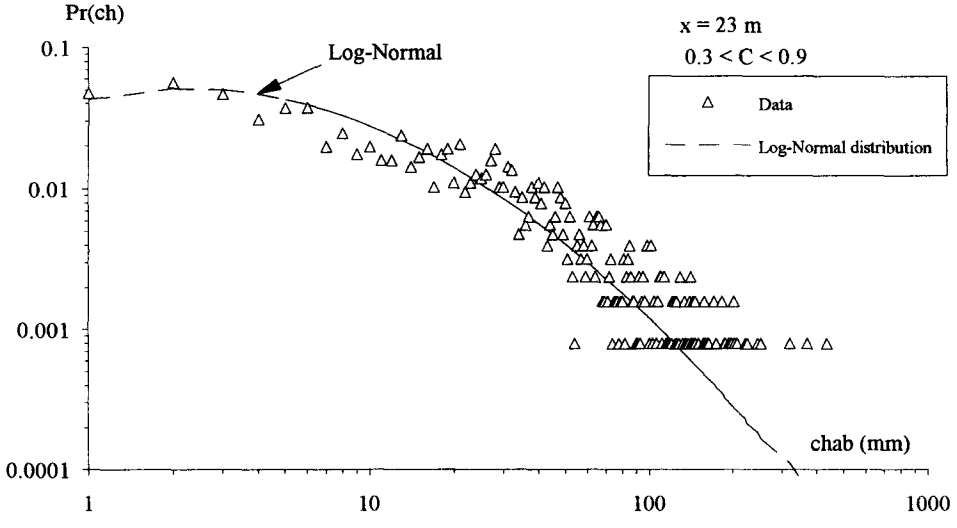

Figure 6. Cumulative bubble chord length histograms at the channel end (Run PDC1, $x = 23$ m). $x = 23$ m, $C_{mean} = 0.09$, $Y_{90} = 0.0481$ m, $V_{90} = 3.76$ m/s, $y(C = 0.3) = 0.0426$ m.

4.2. Cumulative bubble chord length distributions

Cumulative bubble chord length probability histograms are presented in figure 6. The cumulative bubble size distributions were analysed for the bubbly flow and highly-aerated flow separately. The data were compared with normal, gamma, log–normal and Poisson distributions. The log–normal distribution provides the best fit, confirmed by a χ^2 goodness of fit test (Spiegel 1972), in both the bubbly and highly-aerated flow regions.

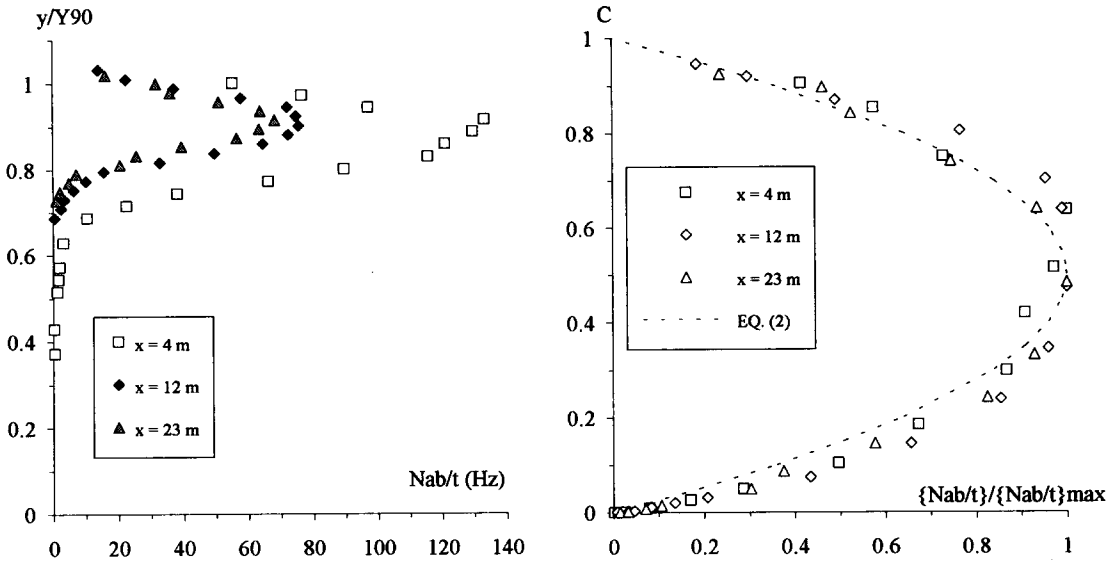

Figure 7. Air bubble frequency in self-aerated open channel flow. Left: (A) Air bubble frequency distribution as a function of the distance from the channel bottom; right: (B) Dimensionless bubble frequency $f_{ab} = F_{ab}/(F_{ab})_{max}$ as a function of the air concentration.

Data are plotted in figure 6(A) for $C < 0.3$ and (B) for $0.3 < C < 0.9$. In figure 6, the data points represent each the probability of a bubble chord length in 1 mm intervals.

It is worth noting that the chord length probability histograms are best fitted by the same type of distributions (i.e. log–normal) in both the bubbly-flow and highly-aerated flow regions.

4.3. Air bubble frequency

At each $\{x,y\}$ position, the air–water mixture can be described also in terms of the air bubble frequency F_{ab}. Data are presented in figure 7 where $F_{ab} = N_{ab}/t$, $f_{ab} = F_{ab}/(F_{ab})_{max}$, and $(F_{ab})_{max}$ is the maximum bubble frequency in the cross-section (table 2).

At each cross-section, the bubble frequency profiles exhibit a maximum $(F_{ab})_{max}$ at about 50% air content (table 2), and they tend towards zero at very-low and very-large air contents (figure 7). Volkart (1980) observed air–water projections with a stroboscopic light. He indicated that "these processes showed frequencies of 46–56 Hz". His observations are of the same order of magnitude as the author's results in the upper flow region (figure 7(A)). Overall the dimensionless air bubble frequency distributions are best correlated by a parabolic function:

$$f_{ab} = 1 - \frac{1}{4}(C - 0.5)^2 \qquad [2]$$

with a coefficient of correlation of 0.9898 (figure 7(B)).

Table 2. Characteristic parameters of air bubble frequency distribution (Run PDC1)

Parameters (1)	Data $x = 4$ m (2)	Data $x = 12$ m (3)	Data $x = 23$ m (4)	Comments (5)
Air–water flow properties				
Y_{90}	0.035	0.0466	0.04811	m
V_{90}	5.03	5.24	3.76	m/s
C_{mean}	0.123	0.096	0.086	Mean air concentration defined in term of Y_{90}
Bubble fequency parameters				
$(F_{ab})_{max}$	133.2	75.6	68.4	Hz (maximum bubble frequency)
$C(F_{ab} = (F_{ab})_{max}$	0.637	0.474	0.484	Local air concentration at maximum bubble frequency location
y/Y_{90} $(F_{(ab)} = (F_{ab})_{max})$	0.914	0.901	0.915	Dimensionless distance where F_{ab} is maximum

4.4. Discussion

The mean chord length size is related to the air content, velocity and bubble frequency by:

$$(ch_{ab})_{NMS} = \frac{CV}{F_{ab}} \quad [3]$$

where $(ch_{ab})_{NMS}$ is the number mean chord length size. Equation [3] is valid for any bubble size shape, bubble size distribution and chord length distribution. It can be used to check the consistency of the bubble analysis. In the present study the data gave consistently: $(ch_{ab})_{NMS}/(CV/F_{ab}) = 0.9830$ for $0.02 < C < 0.98$, with a coefficient of correlation of 0.9714.

5. CONCLUSION

New air bubble measurements were performed in a high-velocity open channel flows. The experimental results show smooth and continuous distributions of void fraction velocity and bubble frequency between 0 and 90% of air content. Bubble chord length results indicate a broad spectrum of entrained air bubble sizes extending over several orders of magnitude (figure 5).

It is suggested that the air–water flow comprises a lower bubbly flow region and a highly-aerated flow region above. In the high-air content regions, air–water projections and foam structures exist as instantaneous structures which constantly evolve in shapes and sizes with time. These are not often seen by eye.

The cumulative bubble chord length distributions are best fitted by log–normal distributions. The bubble frequency distributions follow a simple parabolic centred around $C = 0.5$ [2]. Additional experimental data are required to extend the description of the air–water flow.

Acknowledgements—The author acknowledges the assistance of Ms J. Patterson, Mr M. Mendel and Dr P. D. Cummings. The research project is supported by the Australian Research Council (Ref. A89331591).

REFERENCES

Cain, P. (1978) Measurements within self-aerated flow on a large spillway. Ph.D. thesis, Ref. 78-18, Dept. of Civil Engrg, Univ. of Canterbury, Christchurch, New Zealand.

Chanson, H. (1988) A study of air entrainment and aeration devices on a spillway model. Ph.D. thesis, Ref. 88-8, Dept. of Civil Engrg, University of Canterbury, New Zealand.

Chanson, H. (1993) Self-aerated flows on chutes and spillways. *J. Hyd. Engrg, ASCE* **119,** 220–243. Discussion: **120,** 778–782.

Chanson, H. (1994) Drag reduction in open channel flow by aeration and suspended load. *J. Hyd. Res., IAHR* **32,** 87–101.

Chanson, H. (1995) Air bubble entrainment in free-surface turbulent flows. Experimental investigations. Report CH46/95, Dept. of Civil Engineering, University of Queensland, Australia, June, 368 pp.

Chanson H. and Cummings, P. D. (1996) Air–water interface area in supercritical flows down small-slope chutes. Research Report No. CE151, Dept. of Civil Engineering, University of Queensland, Australia, Feb., 67 pp.

Falvey, H. T. (1980) *Air–Water Flow in Hydraulic Structures*. USBR Engrg Monograph, No. 41, Denver, Colorado, USA.

Halbronn, G., Durand, R. and Cohen de Lara, G. (1953) Air entrainment in steeply sloping flumes. *Proc. 5th IAHR Congress*, IAHR-ASCE, Minneapolis, USA, pp. 455–466.

Schlichting, H. (1979) *Boundary Layer Theory*, 7th Edition. McGraw-Hill, New York.

Schwarz, W. H. and Cosart, W. P. (1961) The two-dimensional wall-jet. *J. Fluid Mech.* **10,** 481–495.

Spiegel, M. R. (1972) *Theory and Problems of Statistics*. McGraw-Hill, New York.

Straub, L. G. and Lamb, O. P. (1953) Experimental studies of air entrainment in open-channel flows. *Proc. 5th IAHR Congress*, IAHR-ASCE, Minneapolis, USA, pp. 425–437.

Thandaveswara, B. S. (1974) Self aerated flow characteristics in developing zones and in hyraulic jumps. Ph.D. thesis, Dept. of Civil Engrg, Indian Institute of Science, Bangalore, India, 399 pp.

Volkart, P. (1980) The mechanism of air bubble entrainment in self-aerated flow. *Int. J. Multiphase Flow* **6,** 411–423.

Wood, I. R. (1991) Air entrainment in free-surface flows. IAHR Hydraulic Structures Design Manual No. 4, *Hydraulic Design Considerations*. Balkema Publ., Rotterdam, The Netherlands, 149 pp.